**Peter Martin[1]**
Department of Mechanical, Manufacturing and
Biomedical Engineering,
Trinity College Dublin,
Parsons Building, College Green,
Dublin 2, Ireland
e-mail: pmartin8@tcd.ie

**Stephen Spence**
Department of Mechanical, Manufacturing and
Biomedical Engineering,
Trinity College Dublin,
Parsons Building, College Green,
Dublin 2, Ireland
e-mail: spences@tcd.ie

**Charles Stuart**
Department of Mechanical, Manufacturing and
Biomedical Engineering,
Trinity College Dublin,
Parsons Building, College Green,
Dublin 2, Ireland
e-mail: stuartch@tcd.ie

**Thomas Leonard**
IHI Charging Systems International GmbH,
Heidelberg 69126, Germany
e-mail: t.leonard@ihi-csi.de

**Andre Starke**
IHI Charging Systems International GmbH,
Heidelberg 69126, Germany
e-mails: a.starke@ihi-csi.de;
andre.starke@accelleron-industries.com

**Marco Geron**
School of Mechanical and Aerospace Engineering,
Queen's University Belfast,
Ashby Building,
Belfast BT9 5AH, UK
e-mail: marco.geron@icloud.com

# Investigating the Suitability of Multi-Scroll Volutes for Improving Spanwise Incidence of Mixed Flow Turbine Rotors With Varying Blade Cone Angles in Automotive Turbocharging Applications

*Targets to reduce fuel consumption and reduce $CO_2$ emissions have been met using engine downsizing and turbocharging. In automotive applications, it is important that the turbocharger responds well to transient events and operates efficiently at both the design and off-design conditions. A mixed flow turbine (MFT) is not constrained to a radial inlet blade angle, allowing the peak efficiency to be shifted to a lower $U/C_{is}$, providing additional freedom to the designer. As the MFT leading edge varies in radius, the spanwise incidence angle also varies, leading to additional separation on the suction surface (SS) of the blade near the hub because of increasingly positive incidence, which is most noticeable at off-design conditions. A multi-scroll volute was previously paired with an MFT with a 45-deg blade cone angle ($\Lambda$), which generated a non-uniform spanwise flow that improved efficiency at off-design at the cost of peak efficiency. The current study identified the range of blade cone angles that benefitted from a multi-scroll volute to reduce incidence at the hub region. A numerical investigation was conducted, which determined the influence a multi-scroll volute can have on MFTs with varying levels of blade cone angle. When the MFT with a large blade cone angle ($\Lambda = 60$ deg) was paired with a multi-scroll volute, the efficiency improved by 2.2%pts at design and 0.5%pts at off-design conditions. The incidence improved, and the mass flowrate increased at the hub region. The MFT with a smaller blade cone angle ($\Lambda = 30$ deg) had performance losses at both operating conditions because the multi-scroll volute increased incidence within the hub region, which reduced the peak efficiency by 1.3%pts. The off-design condition had an excessively positive incidence angle, which was further increased at the hub region by the multi-scroll volute. This resulted in a 0.8%pts reduction in off-design efficiency. The multi-scroll volute concept was shown to offer efficiency improvements for MFTs with larger blade cone angles through better management of the non-uniform spanwise velocity distribution at the rotor inlet.* [DOI: 10.1115/1.4064339]

*Keywords: automotive, turbine, multi-scroll, mono-scroll, volute, MFT, computational fluid dynamics (CFD)*

## 1 Introduction

Radial turbines are ubiquitous in automotive turbocharging applications. The turbocharger is now relied upon to improve the power output of the engine across a wide range of operating conditions, which can be defined through the velocity ratio ($U/C_{is}$). Radial turbines are constrained to achieve peak performance at relatively high $U/C_{is}$ conditions ($U/C_{is} = 0.707$) [1]. A method of reducing the $U/C_{is}$ at which peak efficiency can be achieved is through the introduction of a non-zero inlet blade angle ($\beta_b$).

A radial rotor is constrained to a zero inlet blade angle as a departure from the radial fiber results in excessive stress, compromising the mechanical integrity of the rotor. Mixed flow turbine (MFT) rotors can achieve a non-zero inlet blade angle and still maintain a radially fibered blade [1]. A MFT has an axial velocity component, which experiences the camber angle of the blade ($\Phi$). The blade angle the flow experiences is, therefore, a function of the blade camber angle and flow cone angle ($\lambda$), as shown in Eq. (1) [1].

The blade camber angle can be varied without departing from a radially fibered blade, which allows the MFT to have a non-zero inlet blade angle without introducing additional stresses.

$$\tan \beta = \tan \cos \lambda \qquad (1)$$

Mixed flow rotors provide additional advantages for an automotive turbocharger as they have reduced rotational inertia due to the reduced radius from the shroud to the hub of the leading edge (LE), creating a blade cone angle ($\Lambda$) in the meridional plane (Fig. 1). The reduction in rotational inertia equates to improved responsiveness to transient events. Rowclawski et al. considered the impact rotor inertia and efficiency had on transient response and found that a 20% reduction in rotor rotating inertia resulted in the same impact on the time to torque as a 5% increase in turbine efficiency [2].

Leonard et al. [3] considered the influence of blade cone angle and inlet blade angle on MFT performance. The blade cone angle resulted in a non-uniform blade speed across the rotor leading edge. Due to the conservation of angular momentum, the absolute circumferential velocity component increased at the hub; this effect, coupled with the lower blade speed toward the hub, resulted in a non-uniform incidence angle ($i$) with a more positive incidence angle at the hub region of the MFT. As the blade cone angle increased, the non-uniformity of the spanwise incidence increased. An excessively positive incidence angle results in separation on the suction surface (SS) of the rotor blade, as confirmed by Baines and Yeo [4].

Two MFTs in conjunction with radial stators were studied in detail by Leonard et al., the $\Lambda60\beta10$ rotor (60 deg blade cone angle and a 10 deg nominal inlet blade angle) and the $\Lambda30\beta30$ rotor [3]. The $\Lambda60\beta10$ rotor had a 5%pts efficiency improvement over the baseline radial rotor at design conditions due to a more positive incidence angle preventing separation on the pressure surface (PS). At off-design conditions, the $\Lambda60\beta10$ rotor incurred a highly positive incidence angle, resulting in flow separation on the SS of the rotor blade. The separation caused a flow blockage, greatly reducing the performance of the rotor. The $\Lambda60\beta10$ rotor offered additional benefits with a 46% inertia reduction compared to the baseline radial rotor, making it a highly responsive turbine during turbocharger transients. The $\Lambda30\beta30$ MFT had a 2%pts reduction in efficiency at the design condition. However, at off-design conditions, the $\Lambda30\beta30$ had a 2.1%pts improved efficiency.

Methods to improve the spanwise incidence angle of MFTs have been investigated by altering the MFT geometry and by improving flow conditions upstream of the MFT. Abidat et al. designed two MFTs, one with a constant blade angle (rotor A) and another with

a constant incidence angle (rotor B), by varying the inlet blade angle [5]. The constant blade angle rotor achieved an efficiency 7%pts greater than the constant incidence rotor at $U/C_{is} = 0.64$. The rotors had the same exducer geometry; however, the constant incidence rotor had a reduced axial length, and so the results could not be compared directly. Arcoumanis et al. [6] studied a further MFT, a modified Rotor B with two fewer blades. Laser Doppler velocimetry was used to measure flow field conditions at the inlet and exit. The constant blade angle MFT produced a greater efficiency than the constant incidence angle MFTs. As the axial length and blade number were reduced, it was difficult to directly compare the rotors. Arcoumanis et al. recommended further work developing a volute that would provide a flow that aligned with the rotor blade [6].

Pathways to improve flow conditions upstream of the MFT rotor can be simplified into two categories: the first is aligning the flow of an MFT to have a constant vaneless space from hub to shroud. The second approach is to generate a non-uniform spanwise flow at the stator outlet. This is a more practical approach to improve flow conditions in a turbocharger application as it avoids the potential for a leaned volute to clash with the bearing housing. A numerical study by Lee et al. [7] used a tilted mono-scroll housing, which improved the SS separation in the MFT, increasing the efficiency by 1.2%pts. This followed the suggestion of Arcoumanis et al. [6] to develop a volute that aligned the flow with the blade in the meridional plane. The tilted housing was numerically evaluated under steady-state and pulsating flow conditions. In practical turbocharger applications, the angle the volute could be tilted to would be limited by the bearing housing and avoiding increasing the shaft length.

The generation of a non-uniform spanwise flow has been investigated by both Lee et al. [8] and Morrison et al. [9–11]. This is a more practical approach to improve flow conditions in a turbocharger application. Lee et al. imposed velocity components at the inlet of a MFT. Five different distributions of spanwise velocity were imposed, achieving up to 2.17%pts efficiency gains [8].

Morrison et al. [10] generated a non-uniform spanwise flow by a set of leaned stator vanes. The leaned stator vanes improved performance across the entire operating range, with a maximum performance improvement of 5%pts [10]. Although the leaned stator vanes generated a non-uniform spanwise flow and improved the performance, the vanes were fixed, complex, and not feasible for serial production for an automotive turbocharger application.

In a numerical study, Morrison et al. [11] introduced the multi-scroll volute and paired it with the $\Lambda45\beta20$ MFT. The multi-scroll design also generated a non-uniform spanwise flow, which improved the incidence at the hub of the MFT. The study showed that the multi-scroll volute could overcome the additional losses associated with the inclusion of a meridional divider, which was first reported by Capobianco and Gambarotta comparing twin-scroll and mono-scroll volutes [12]. The meridional divider increased the wetted surface area compared to the mono-scroll, leading to additional frictional losses. In addition to the increased surface area, the multi-scroll meridional divider introduced a wake. Morrison et al. achieved a 2.2%pts efficiency gain at the off-design condition at the expense of a 0.6%pts efficiency loss at the design condition when using a multi-scroll volute [11].

The multi-scroll volute can be advantageous to turbocharger designers as it is a more feasible design for serial production and provides a variable geometry option through the implementation of partial admission. Morrison et al. did not consider the impact of varying blade cone angles and whether the multi-scroll would be able to generate a flow field that improved performance for large and small blade cone angles.

As a result of the work conducted by Leonard et al. and Morrison et al., further work with the multi-scroll concept is required with MFTs of different blade cone angles. This study addresses the following questions:

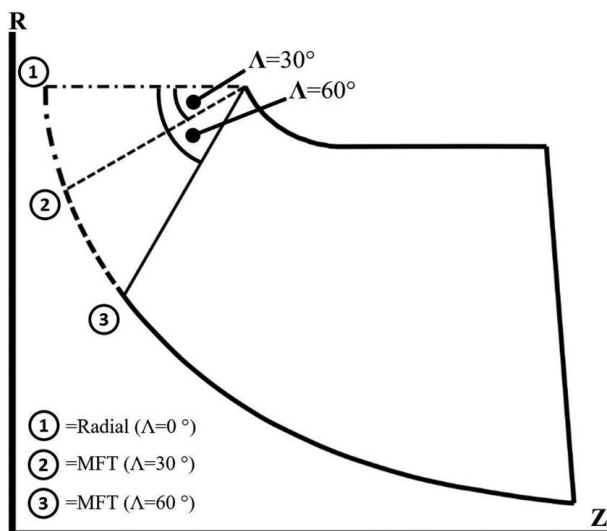(1) Can the multi-scroll volute produce an efficiency improvement for large or small cone angle MFTs, or both?



**Fig. 1  Blade cone angles**

(2) Can the multi-scroll volute improve efficiency at the off-design condition without sacrificing peak efficiency, and how does this vary for different MFT blade cone angles?

(3) How can the design parameters of the multi-scroll volute be varied to optimize the flow field at the rotor inlet, and what are the flow physics underlying the changes in flow field and MFT performance?

Following the justification of Leonard et al. [3], the $\Lambda60\beta10$ and $\Lambda30\beta30$ MFTs were used in this study. These rotors had significantly different blade cone angles ($\Lambda$) and offered efficiency gains at different operating conditions. The $\Lambda60\beta10$ also had a significant inertia reduction. A numerical analysis was conducted on a design matrix of 24 different multi-scroll volute geometries to understand their performance influence on two different MFT cone angles. The numerical model was validated from previous experimental testing of the $\Lambda30\beta30$ MFT.

The paper is subdivided into four sections. The first section introduces the impact on the performance of the blade cone angle and the potential for the multi-scroll volute to modify the rotor flow field. Section 2 details the multi-scroll volute geometry and the methodology used to conduct this work. Section 3 describes the numerical model used throughout the study and how the model was validated. Section 4 analyzes the results to understand the impact the multi-scroll volutes had on the $\Lambda60\beta10$ and $\Lambda30\beta30$ MFTs. The study focused on two operating points: a design point and a lower efficiency off-design condition. The underlying flow physics have been presented to explain why the $\Lambda60\beta10$ MFT had a greater efficiency improvement at design conditions and why the $\Lambda30\beta30$ MFT had reduced efficiency at all operating conditions.

## 2 Methodology

**2.1 Multi-Scroll Volute Concept and Design.** The multi-scroll volute design described by Morrison et al. [11] is similar to a conventional twin-scroll volute; however, the way in which the exhaust gas from the engine is fed between the two limbs is different. The twin-scroll volute has two separate supplies from the exhaust manifold; each manifold supply feeds one of the limbs of the volute to make the best use of the pulse energy in the exhaust flow. The multi-scroll volute is fed like a mono-scroll volute, where the flow is supplied to both limbs by one common manifold inlet. The exhaust gas flow is then divided between the two limbs through the meridional divider alone (Fig. 2).

The multi-scroll has, therefore, been designed to replace a mono-scroll volute paired with a mixed flow rotor. This is achieved by altering the distribution of volute flow and outlet areas between the hub and shroud limbs, as presented in Fig. 3. The multi-scroll volute does not divide the flow to extract more energy from the exhaust pulses and, therefore, is not directly comparable with a twin-scroll or double-scroll volute.

The cross section of the multi-scroll volute has three main regions: the flow areas (FA), the outlet areas (OA), and the mixing region area (Fig. 3). The flow area and outlet area can
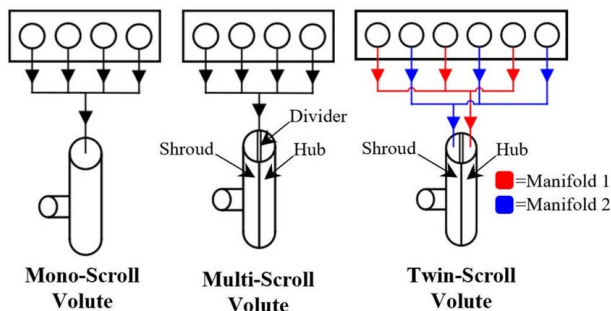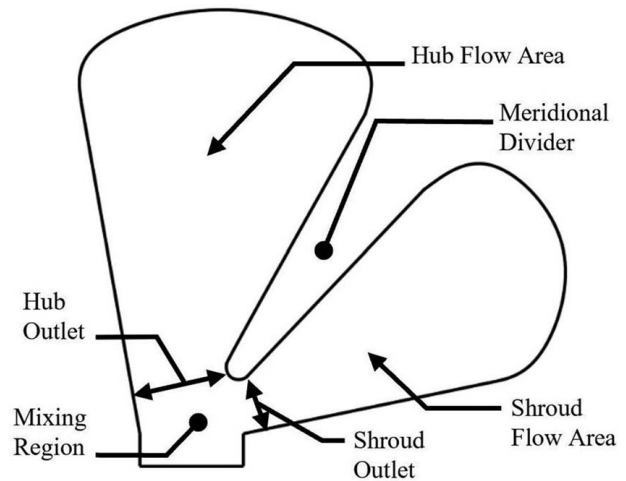


**Fig. 3  Multi-scroll regions**

then be subdivided into their respective hub or shroud side counterparts. The naming convention adopted for different multi-scroll volutes in this study was %FA$_{hub}$_%OA$_{hub}$, where %FA$_{hub}$ was the percentage of the flow area of the hub limb relative to the total flow area of the hub and shroud limbs. Similarly, the %OA$_{hub}$ was the percentage of the outlet area of the hub limb relative to the total outlet area of the hub and shroud limbs combined. The expressions to calculate these variables are provided in Eqs. (2) and (3).

$$\%FA_{hub} = \frac{FA_{hub}}{FA_{hub} + FA_{shroud}} \times 100 \qquad (2)$$

$$\%OA_{hub} = \frac{OA_{hub}}{OA_{hub} + OA_{shroud}} \times 100 \qquad (3)$$

The multi-scroll volute was created as a parametric surface model. To limit the number of design variables used in conducting the volute study, only the limb radii and the position of the meridional divider tip in the axial and radial direction were varied to generate a range of multi-scroll profiles, as illustrated in Fig. 4. All angles in Fig. 4 were kept constant.

The multi-scroll volutes in this study were designed to have a profile similar to that of a modern automotive turbocharger and, therefore, the evenly distributed profile (50_50) was not a symmetric profile (Fig. 4). This is largely due to the strict packaging constraints of an automotive turbocharger.

**2.2 Study Methodology.** The study investigated a wide range of multi-scroll volute designs, with a focus on the spanwise non-
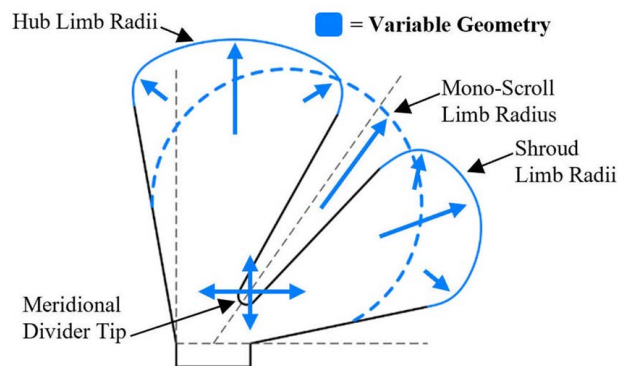


**Fig. 2  Volute exhaust gas supply from manifold**



**Fig. 4  Multi-scroll and mono-scroll parameters**

**Table 1  Multi-scroll design matrix**

| | | Hub limb flow area, $FA_{Hub}$ (%) | | | |
|---|---|---|---|---|---|
| | | 50 | 60 | 70 | 80 |
| Hub outlet area, $OA_{Hub}$ (%) | 30 | 50_30 | 60_30 | 70_30 | 80_30 |
| | 40 | 50_40 | 60_40 | 70_40 | 80_40 |
| | 50 | 50_50 | 60_50 | 70_50 | 80_50 |
| | 60 | 50_60 | 60_60 | 70_60 | 80_60 |
| | 70 | 50_70 | 60_70 | 70_70 | 80_70 |
| | 80 | 50_80 | 60_80 | 70_80 | 80_80 |



**Fig. 5  Multi-scroll *A/r* distribution**

**Table 2  Turbine operating conditions**

| Operating condition | $T_{01}$ (K) | Pressure ratio | $N$ (rpm) | $U/C_{is}$ |
|---|---|---|---|---|
| Design | 410 | 2.2 | 61,000 | 0.709 |
| Off-design | 410 | 2.0 | 27,100 | 0.327 |

uniformity of the flow field at the rotor inlet, particularly at the hub region, which had the highest incidence. As the study aimed to identify the range of blade cone angles that could benefit from a multi-scroll volute through improved spanwise incidence, the $\Lambda30\beta30$ and $\Lambda60\beta10$ rotors previously studied by Leonard et al. [3] were used in this research. The MFTs comprised nine blades and were scaled from an automotive turbocharger to a shroud tip diameter of 90 mm. A parametric study was conducted to investigate the multi-scroll volute designs. A range of differing flow area and outlet area variations were generated and compiled into a design matrix comprising 24 different volutes, which is given in Table 1. Each multi-scroll volute in the design matrix was numerically evaluated for each of two different turbine rotors at two different operating conditions, specified in Table 2. The design condition was approximately the best efficiency point and corresponded to a $U/C_{is}$ value of 0.709 based on the blade speed at the rotor shroud tip radius. The off-design point was at a considerably lower shaft speed and a $U/C_{is}$ value of 0.327. The rotor shroud tip radius was used to compute the $U/C_{is}$ value in this case because the root-mean-square (RMS) radius at the LE of the MFT rotors varied due to the change in blade cone angle, and using the mean radius at the LE would have produced different $U/C_{is}$ values for the same pressure ratio and shaft speed. Using a $U/C_{is}$ value at the shroud tip allows direct comparison with a radial turbine rotor of the same diameter and speed.

The total critical flow area just above the trailing edge (TE) of the volute tongue and the total outlet areas were kept consistent throughout the volute designs to prevent mass flow changes between designs occurring from an increased area rather than through alterations of aerodynamic blockage. The *A/r* varied throughout the design matrix as a consequence of altering the flow area distribution in each limb and inevitably the centroid of each limb cross section too (Fig. 5). As an example, Fig. 6 shows the profile differences between the 50_50 and 80_80 multi-scroll volutes.

A mono-scroll volute was used as a baseline case to compare the performance of the multi-scroll volutes. The mono-scroll volute followed the same design constraints as the multi-scroll volute. Overhang angles, volute outlet diameter, and outlet height were consistent, and the flow area of the mono-scroll was varied by adjusting the limb radius only. A comparison between the multi-scroll and mono-scroll cross-sectional profiles is provided in Fig. 4.

## 3  Numerical Model

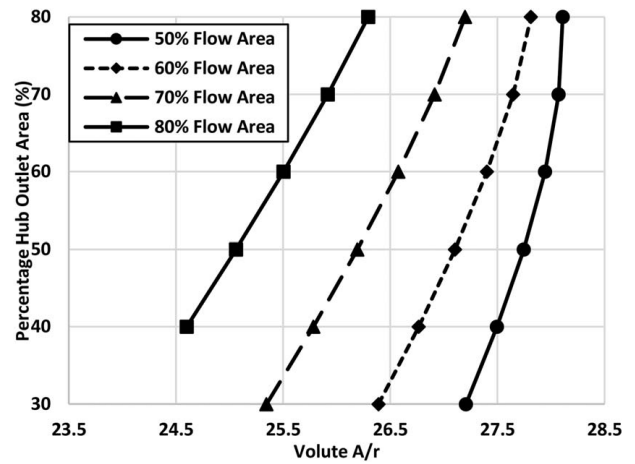**3.1  Numerical Model Configuration.** The numerical model was constructed using the commercial software ANSYS CFX 2019R3. The numerical model was configured as a steady-state model utilizing the Reynolds-averaged Navier–Stokes equations. The shear stress transport (SST) turbulence model was chosen as previous studies have shown good agreement with experimental results [3,10,13]. The numerical model was set up to represent the experimental test rig used in Refs. [3,10,13], where the inlet conditions were specified as total temperature ($T_{01}$) and total pressure ($P_{01}$), while outlet conditions were specified as average static pressure at the diffuser outlet ($P_4$).

The model consisted of four domains; the volute, rotor, backdisk cavity, and exhaust diffuser. The study investigated the flow field at the hub region of the rotor leading edge; therefore, the inclusion of the backdisk cavity was necessary in the computational domain. All components were meshed using ANSYS Turbogrid or ANSYS ICEM-CFD with an average $y^+$ below 2 and a maximum $y^+$ of 5. This is more than sufficient for the SST turbulence model, which requires a $y^+$ value of less than 11 [14–16]. The diffuser, rotor, and backdisk cavity meshes comprised structured hexahedral cells. The diffuser mesh was previously generated by Leonard et al. [3], where it was subjected to a grid independence study and experimental validation.

The rotor and the backdisk cavity meshes were modeled as separate components. To incorporate the backdisk into the CFD model, the rotor was divided into two domains—the inlet and passage domains, as labeled in Fig. 7. A 1:1 interface between the inlet
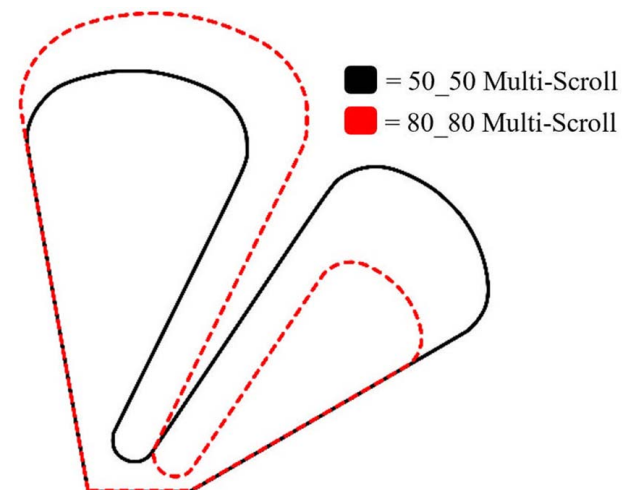


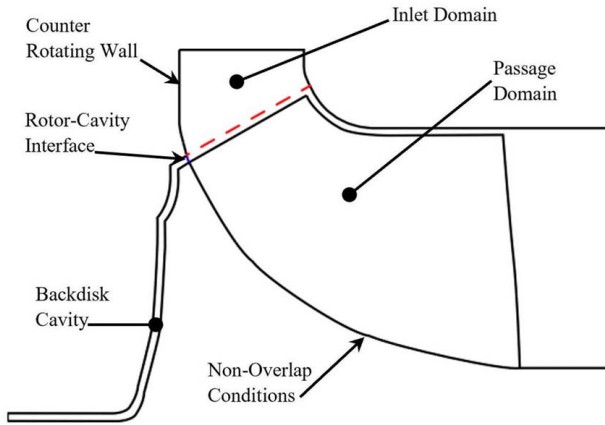**Fig. 6  50_50 versus 80_80 cross sectional profile**

**Fig. 7  Rotor–cavity detail**



**Fig. 9  Meridional section of computational model**

domain and passage domain was located at the start of the backdisk cavity. The cavity mesh was included within the rotor passage domain to avoid highly skewed cells at the rotor leading edge and improve the overall mesh quality. A general grid interface (GGI) connection was utilized for the rotor–cavity interface. To enable flow to pass between the rotor and cavity, the whole rotor hub was included in this interface, and a non-overlap condition was applied to replicate a physical hub wall of the rotor, details of which are shown in Fig. 7.

The volute meshes consisted of unstructured tetrahedral cells with 15 layers of prism cells to better capture the boundary layer. Different mesh regions were utilized to achieve a finer mesh prior to the limb outlets, continuing to the volute outlet, as shown in Fig. 8.

To reduce computational cost, only the volute was included as a full 360-deg domain. The remaining components were incorporated as single blade passage segments. A mixing plane interface was employed between the volute outlet and rotor inlet, located at 112% of the rotor shroud tip radius. The velocity downstream of the mixing plane was calculated using the constant total pressure method. This option is recommended for closely coupled components and has found good agreement with previous experimental validation [3,10]. As a mixing plane interface was used between the volute outlet and rotor inlet, it must be acknowledged that the impact from the volute tongue on the rotor flow field would be lost. Considering the large number of turbine cases simulated in this study (96 simulations presented here), it was necessary to control the overall computational cost; this compromise was deemed acceptable as the volute tongue geometry was consistent throughout all volutes and the impact of the mixing plane would, therefore, be consistent and allow comparison between different cases.
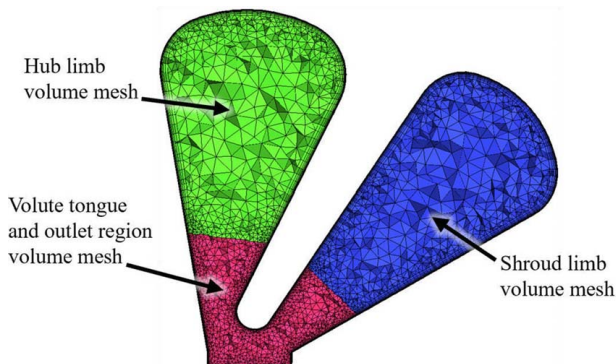


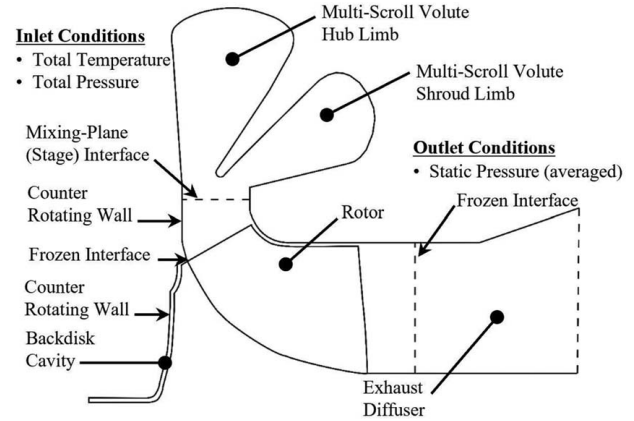**Fig. 8  Multi-scroll mesh cross section**

To ensure the compromise was suitable, a full 360-deg setup was created. This modeled a full rotor, backdisk cavity, and exhaust diffuser with multiple reference planes used throughout, including the volute-rotor connection. Two clocking angles between the rotor and volute were used. There was a 1.6% difference in efficiency at design and 0.4% at off-design conditions between the averaged 360 models and the mixing plane model. The 50_30 multi-scroll case was paired with the Λ60β10 rotor while comparing both models.

The remaining components used a multiple reference frame interface. No-slip, adiabatic, smooth wall conditions were applied to all walls, neglecting material surface roughness in this study. A meridional profile of the computational domain is provided in Fig. 9.

The numerical simulation was deemed sufficiently converged when the RMS residuals reached a value below $1 \times 10^{-4}$, efficiency varied by less than 0.01%pts over 200 iterations, and the mass flow varied by less than 0.001% over 200 iterations. Although the criterion for residuals was set to $1 \times 10^{-4}$, the majority of simulations converged with residuals below $1 \times 10^{-5}$.

**3.2  Grid Independence.** A comprehensive grid independence study was conducted following the Grid Convergence Index (GCI) method, initially introduced by Roache [17]. The GCI method has evolved, and for clarification, this study followed the method outlined by Celik et al. [18]. The GCI method provides a systematic approach to investigating grid independence whereby three or more meshes have their cell count scaled according to Eq. (4). The refinement factor ($r_f$) was targeted as 1.4 throughout the entire grid independence study. All components in this study were three-dimensional; therefore, the dimension (D) was set as three for the entire study. Ideally, the grid topology is kept as consistent as possible to ensure accurate refinement and confidently confirm that increasing the grid density further does not improve numerical accuracy.

$$r_f = \left[ \frac{\text{Total Element Number}_{\text{Fine}}}{\text{Total Element Number}_{\text{Coarse}}} \right]^{1/D} \qquad (4)$$

Approximate relative errors ($e_a$) of the mass flow parameter (MFP) and total-to-static efficiency were determined between the two corresponding mesh densities. This approximate relative error was then used in Eq. (5) to determine the GCI level of uncertainty for each performance parameter. The Factor of Safety (FoS) was set as 1.25, and the apparent order of convergence ($p$) was determined.

$$\text{GCI} = \frac{\text{FoS}e_a}{r_f^p - 1} \qquad (5)$$

The grid was judged suitably independent when the GCI level of uncertainty was equal to or less than the level of uncertainty from

| Variable | Experimental uncertainty |
|---|---|
| Efficiency (design) | 0.20%pts |
| Efficiency (off-design) | 0.12%pts |
| MFP | 0.56% |
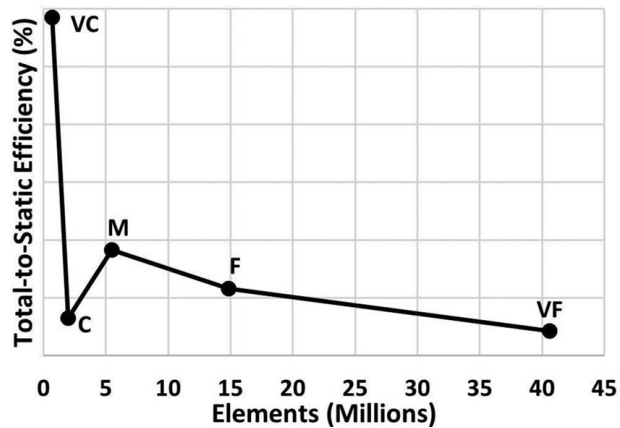


Fig. 10    Grid convergence graph of 50_50 multi-scroll volute



Fig. 11    Numerical model of test rig configuration

previous experimental testing (Table 3). The GCI method was used for the volute, rotor, and cavity meshes. Each domain was considered as a separate case but included all four domains in the numerical model. The mesh density of the domain under investigation was varied, and the remaining domain meshes stayed constant, using the generated "fine" mesh. Any changes in stage performance would, therefore, be a result of adjusting the mesh density of that specific component. Another reason for adopting this approach was that increasing the mesh density of all four components with a refinement factor of 1.4 would result in a numerical model with an extremely high overall cell count that would not be practical to compute. A plot of grid convergence has been provided in Fig. 10.

The GCI method was conducted for both rotors and their respective backdisk cavities. Two configurations of multi-scroll volute were investigated with the GCI method and at both design and off-design conditions. The 50_50 case was chosen as it was proposed to have the least non-uniform flow distribution and behave most like the mono-scroll baseline. The 80_80 multi-scroll volute was also selected as a more extreme case of non-uniformity. Final cell counts of each domain and their numerical uncertainty have been provided in Table 4.

**3.3  Model Validation.** The results from a previous experimental study conducted by Leonard et al. [3] were used to validate

Table 4    Final meshes used

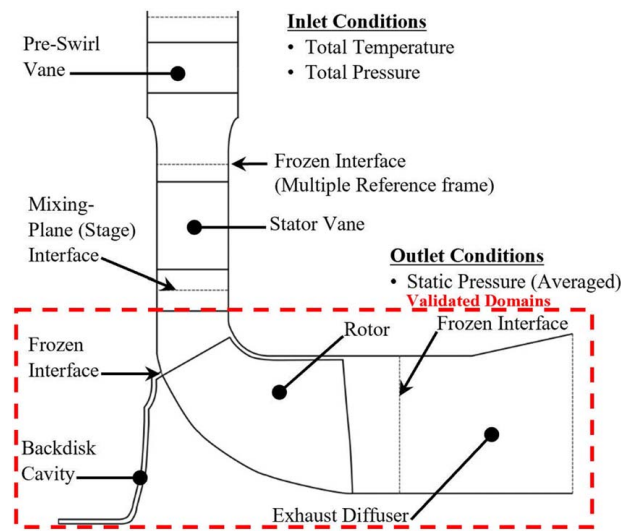| Component | Cell count | GCI $\eta_{TS}$ uncertainty (% pts) | GCI MFP uncertainty (%) |
|---|---|---|---|
| Multi-scroll volute (design) | 14,000 k– 15,000 k | 0.002–0.06 | 0.18–0.29 |
| Multi-scroll (off-design) | 14,000 k– 15,000 k | 0.01–0.1 | 0.12–0.45 |
| Λ30β30 rotor | 2700 k | 0.27 | 0.03 |
| Λ30β30 cavity | 450 k | 0.0004 | 0.02 |
| Λ60β10 rotor | 2700 k | 0.12 | 0.35 |
| Λ60β10 cavity | 450 k | 0.048 | 0.00046 |
| Exhaust diffuser | 250 k | N/A | N/A |

the CFD model. The axisymmetric cold flow test rig used a set of pre-swirl vanes and stator vanes as the swirl-generating component rather than a volute. To validate the CFD model in this study, the pre-swirl and stator vanes were meshed, and a grid independence study was conducted following the GCI method. The numerical model imposed the same modeling conditions as the multi-scroll study (Fig. 11). This method validated the CFD modeling conditions, the rotor mesh, and the exhaust diffuser mesh.

Figure 12 shows the predicted efficiency compared to experimental results for the Λ30β30 rotor case. A maximum discrepancy in efficiency was 2.6%pts at off-design conditions. Figure 13 compares the measured MFP to the predicted one. A maximum discrepancy in MFP of 3.5% occurred at mid-speed conditions (33.9 k rpm). The overall trends of the predicted results followed the measured experimental results, and the rotor and exhaust diffuser meshes of the CFD model were considered sufficiently validated. The multi-scroll volute was not experimentally tested and, therefore, the mesh was not validated; however, the GCI level of uncertainty was below the experimental uncertainty level, and the volute grids were considered acceptable since they followed the same mesh development procedure as the other components that were experimentally validated.
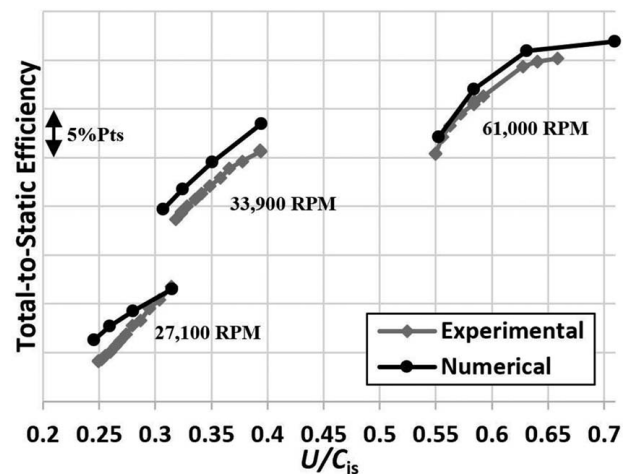


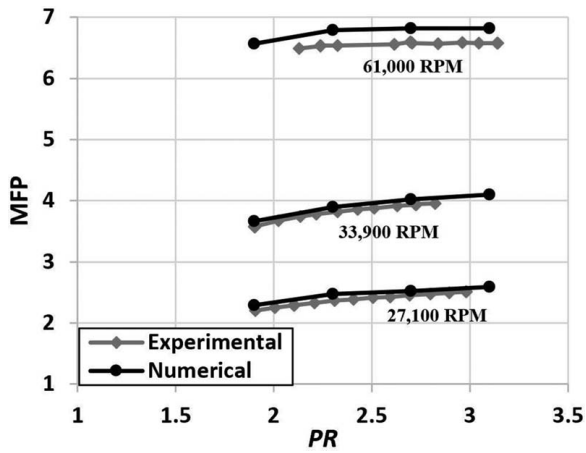Fig. 12    Validation of numerical model $\eta_{TS}$ against experimental results (Λ30β30 rotor)

**Fig. 13 Validation of numerical model MFP against experimental results (Λ30β30 rotor)**

## 4 Results and Discussion

**4.1 Design Matrix Results.** The change in total-to-static efficiency from the baseline mono-scroll case has been included for both rotors at design and off-design operating conditions in Fig. 14. The efficiency calculation was based on static conditions at the diffuser exit. The Λ60β10 MFT efficiency improved with the multi-scroll volute at design (+2.2%pts) and off-design condition (+0.5%pts). None of the multi-scroll volute configurations were able to increase the efficiency of the Λ30β30 rotor at either
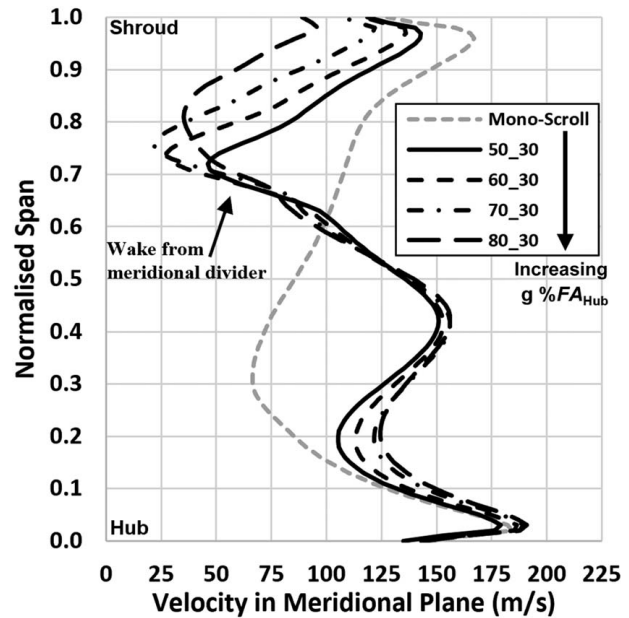


**Fig. 15 Spanwise velocity in meridional plane at the leading edge of the Λ60β10 rotor considering multi-scroll volutes with variable % hub flow area**

operating condition; therefore, further investigation of the Λ30β30 rotor has not been presented in this paper.

When considering the Λ60β10 results, the 50_30 multi-scroll case had a 1.2% greater MFP than the baseline at design condition, and at off-design, the 50_30 multi-scroll case had a 3% increase in MFP.

### 4.2 Λ60β10 Rotor Results

*4.2.1 Influence of Volute Parameters on Rotor Inlet Flow.* The changes to the rotor inlet flow field due to the multi-scroll volute
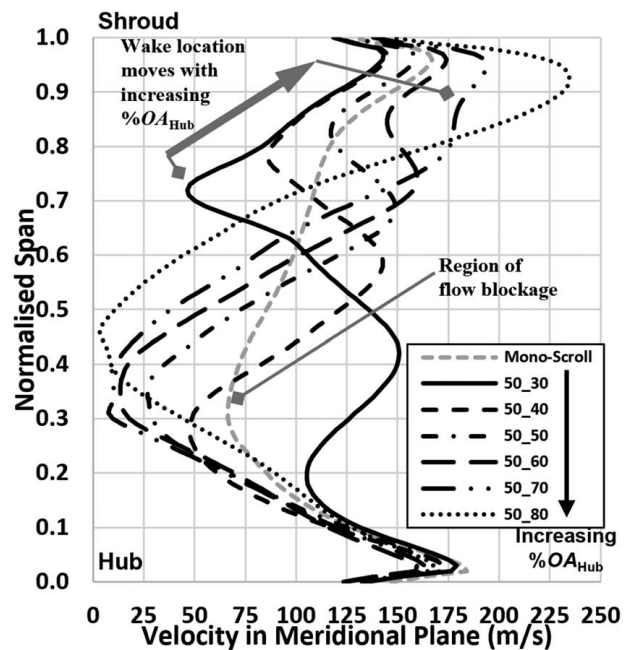


**Fig. 14 Efficiency change of Λ60β10 rotor design matrix**



**Fig. 16 Spanwise velocity in meridional plane at the leading edge of the Λ60β10 rotor considering multi-scroll volutes with variable % hub outlet area**
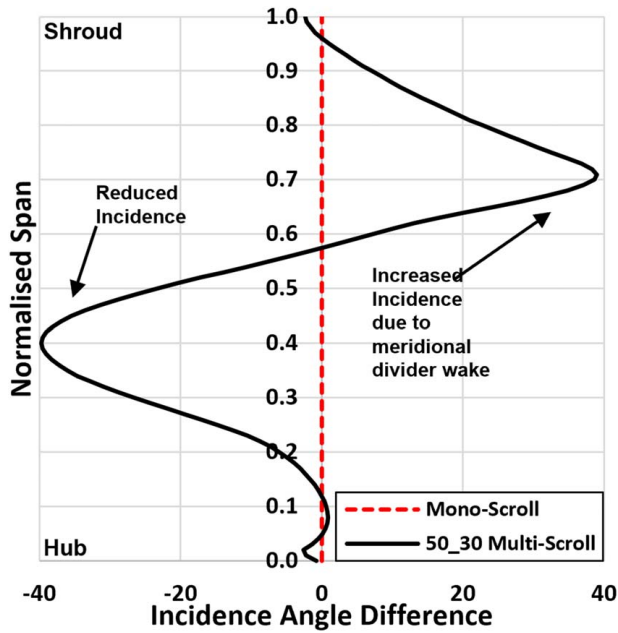
Fig. 17  50_30 multi-scroll incidence angle difference from baseline mono-scroll paired with the Λ60β10 rotor at design condition



Fig. 19  Entropy generation rate of 50_30 multi-scroll (top) and mono-scroll (bottom) at rotor leading edge with the Λ60β10 rotor at design condition

were considered by altering both the limb flow area and outlet area distributions independently to identify which parameter had the greatest impact in manipulating the flow. Pitchwise averaged axial and radial velocity components along the span just upstream of the rotor LE were used to calculate the velocity in the meridional plane, presented in Figs. 15 and 16. Each configuration was considered at the design condition. The grey dashed line represents the velocity profile from the baseline mono-scroll case. Figure 15 shows the impact of adjusting the %hub flow area, $\%FA_{Hub}$, while the outlet area distribution was held constant. Figure 16 shows the impact of adjusting the %hub outlet area, $\%OA_{Hub}$, while the flow area distribution was held constant. The spanwise flow field was clearly more sensitive to changes in the limb outlet
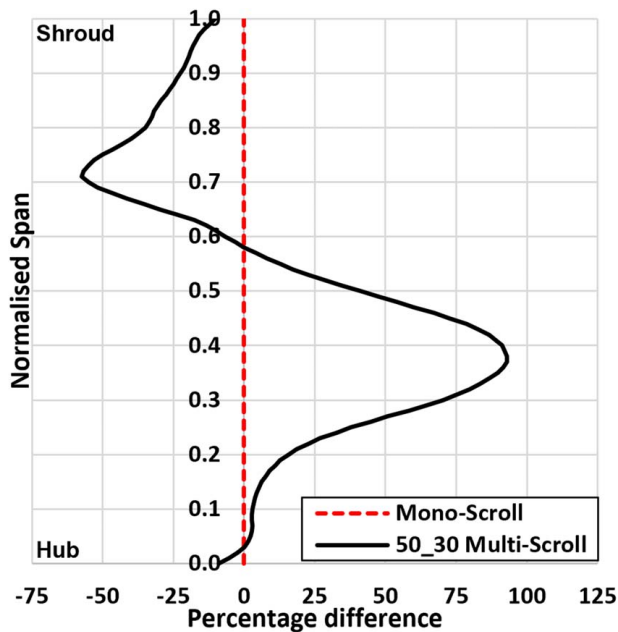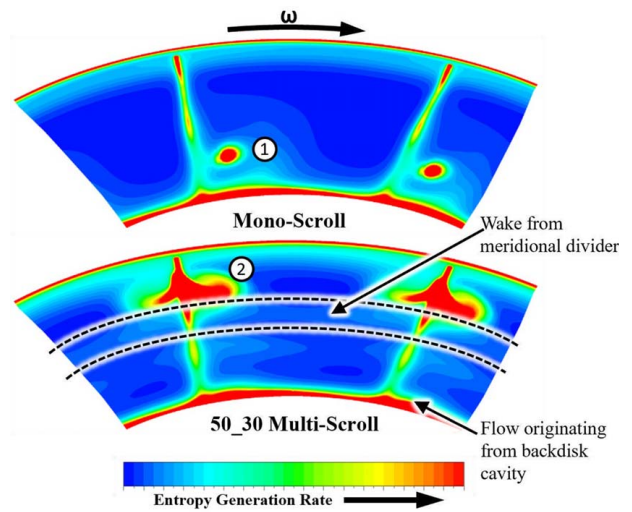
area distribution (Fig. 16) than the flow area distribution (Fig. 15) (note that the abscissa scales are different between Figs. 15 and 16). The lower half of the span was mainly influenced by the limb outlet area. The shroud region experienced greater variation, primarily a reduction in local mass flow as the %hub flow area increased.

Figure 16 shows that the limb outlet area distribution is a far more sensitive parameter to alter the spanwise flow field. An increase in the hub outlet area reduced the mass flow at the hub region and increased the mass flow at the shroud region. The 30% hub outlet area volute (50_30) had the most positive radial velocity at the hub region, indicating a large proportion of the mass flow passed through the hub region. All multi-scroll configurations had evidence of the wake from the meridional divider present, ranging from 70% span up to 90% span (Figs. 15 and 16).

*4.2.2  Design Condition.*  The design condition efficiency of the Λ60β10 MFT showed the greatest improvement with the 50_30



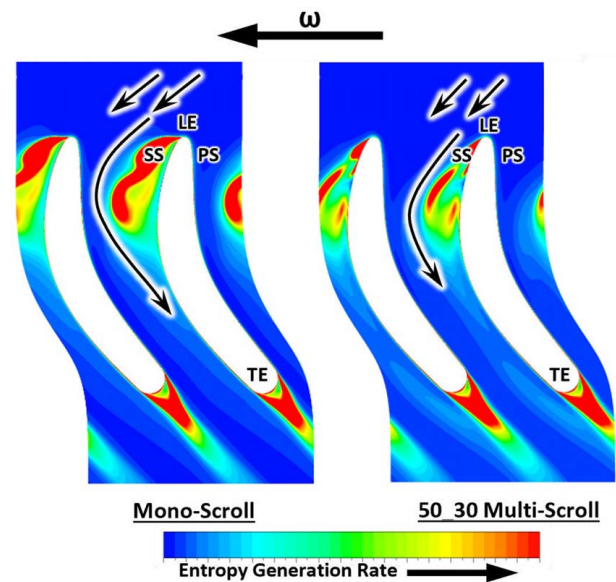Fig. 18  Mass flowrate difference from mono-scroll baseline at rotor leading edge



Fig. 20  Entropy generation rate of mono-scroll (left) and 50_30 multi-scroll (right) cases at 20% span of the Λ60β10 rotor operating at design condition
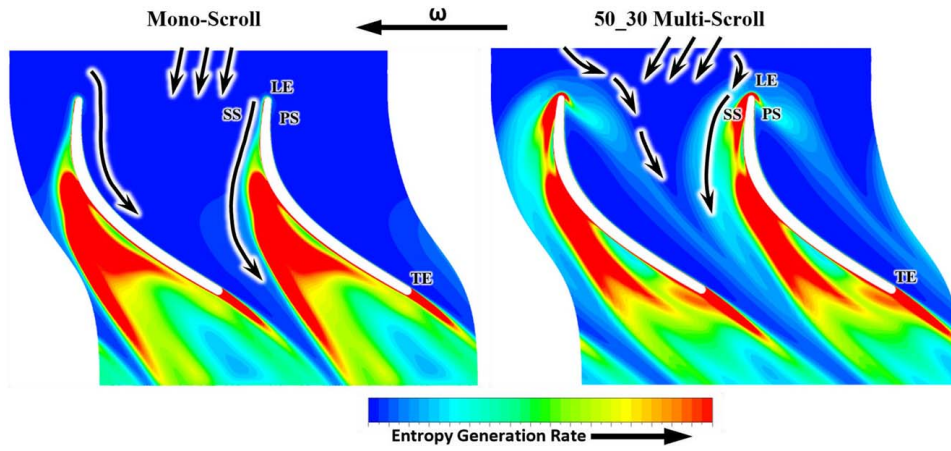
**Fig. 21 Entropy generation rate of mono-scroll (left) and 50_30 multi-scroll (right) case at 80% span of the Λ60β10 rotor operating at design condition**

multi-scroll configuration, with a predicted improvement of 2.2% pts. Therefore, the 50_30 volute configuration was investigated in detail for both the design and off-design conditions of the Λ60β10 MFT.

Figure 17 presents the change in incidence angle across the rotor LE calculated from pitchwise averaged values of the velocity components and the blade geometry. The plot shows the difference in incidence angle between the baseline mono-scroll volute and the 50_30 multi-scroll volute. The incidence angle was substantially reduced around 20–50% span due to the modified flow field from the multi-scroll volute. This improvement in incidence was connected to the redistribution of mass flowrate across the span. The 50_30 multi-scroll volute generated a non-uniform spanwise flow field, distributing more mass flow than the mono-scroll case over the first 50% of the blade span (Fig. 18). The increase in mass flow into the hub region of the rotor was due to improved flow conditions at rotor inlet, and particularly the partial elimination of a region of flow blockage that was present in the Λ60β10 rotor with the baseline mono-scroll at 30% span caused by excessively positive incidence, which can be observed in Fig. 16. The mass flowrate was lower than the baseline for the remaining span. Conversely, the incidence angle in Fig. 17 was increased at the shroud, but there was less mass flow at this region of the rotor LE.

Expressions to evaluate the entropy generation rate were implemented following the method of Kock and Herwig [19]. Figure 19 shows the entropy generation rate in a plane just upstream of the rotor LE. It is apparent that the hub region of loss due to high incidence ① was eliminated in the multi-scroll case; however, a sizable region of loss was introduced within the shroud region ②. This shroud region loss was a consequence of the meridional divider. The wake generated by the divider moved downstream and could be observed in the upper span in Fig. 19, where the flow field was significantly altered, resulting in a highly positive
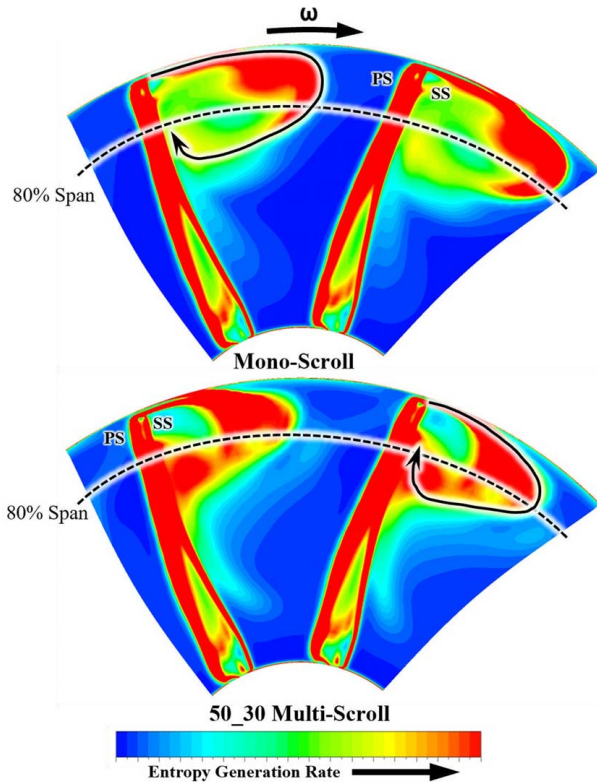


**Fig. 22 Entropy generation rate of 50_30 multi-scroll (top) and mono-scroll (bottom) at rotor trailing edge with the Λ60β10 rotor at design condition**
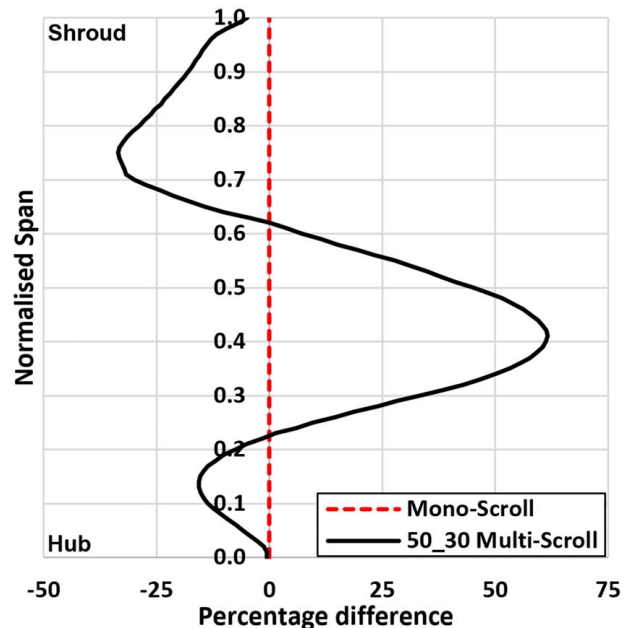


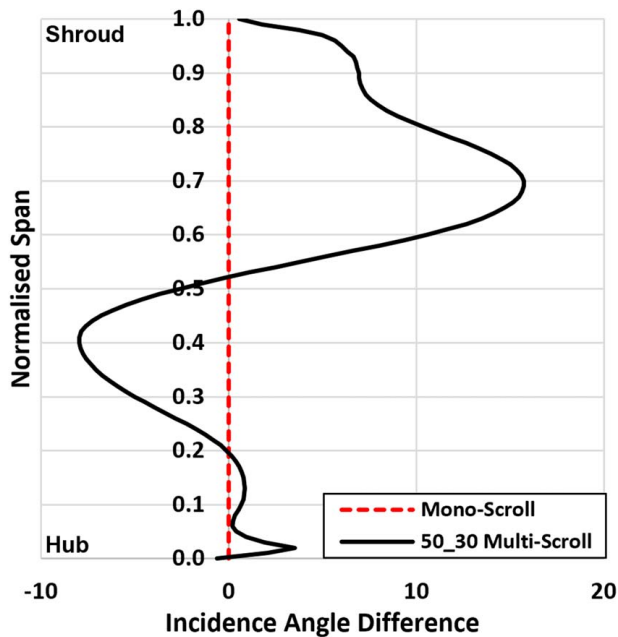**Fig. 23 Mass flow rate difference from mono-scroll baseline at rotor leading edge**

**Fig. 24 50_30 Multi-scroll incidence angle difference from baseline mono-scroll paired with the Λ60β10 rotor at off-design condition**



**Fig. 26 Off-design condition entropy generation rate of 50_30 multi-scroll volute at 30% blade chord**

incidence angle near the shroud. The improved flow field generated by the multi-scroll volute reduced the level of SS separation within the hub region beyond the leading edge. This is observed at 20% span in Fig. 20. This separation is combined with the flow out of the backdisk cavity. As the high-loss flow from the separation moved downstream, it remained close to the SS of the rotor blade. It traveled up the span of the blade toward the shroud, where it interacted with the tip leakage vortex (TLV), generating a large area of aerodynamic blockage.

Looking at the blade passage at 80% span, in Fig. 21, it can be observed that additional loss mechanisms were introduced with the multi-scroll volute case. These additional losses originated
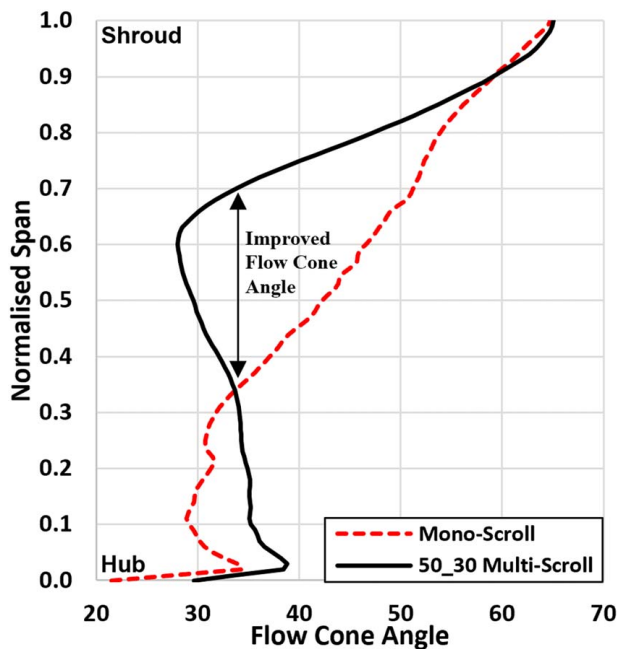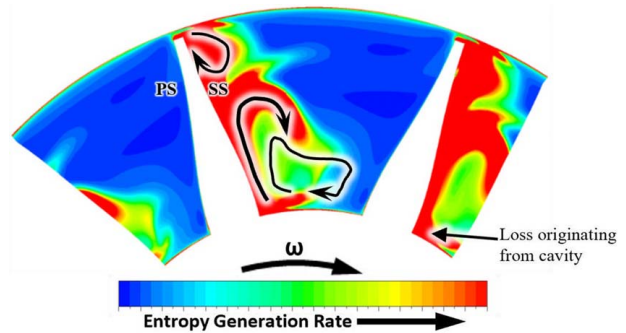
from the excessively positive incidence angle generated by the wake from the meridional divider. This loss moved downstream, combining with SS separation that originated at the hub. The overall loss at 80% span of the rotor passage was less intense for the 50_30 multi-scroll case than for the mono-scroll case since it can be observed that the mono-scroll case experienced a larger area of high levels of entropy generation rate by the time the flow reached the rotor outlet (Fig. 22). Although additional losses were generated at the shroud and mass flowrate of leakage through the blade tip gap was 2% greater for the 50_30 multi-scroll case indicating a greater tip loading, the overall mass flowrate into the rotor from 60% to 100% span was reduced relative to the mono-scroll baseline, as presented in Fig. 18. Therefore, the additional loss regions had a less significant impact on overall performance compared to the improved performance within the hub region. Figure 21 shows the loss region on the SS divides in two directions prior to the TE at 80% span. This phenomenon can be explained by looking at the flow field at the trailing edge in Fig. 22. The two ends of the divided flow were separate sections of the recirculating flow whereby the tip leakage vortex interacted with the high entropy flow that originated from the separation at the hub region at the rotor leading edge.

*4.2.3 Off-Design Condition.* At the off-design condition, the 50_30 multi-scroll configuration achieved an efficiency
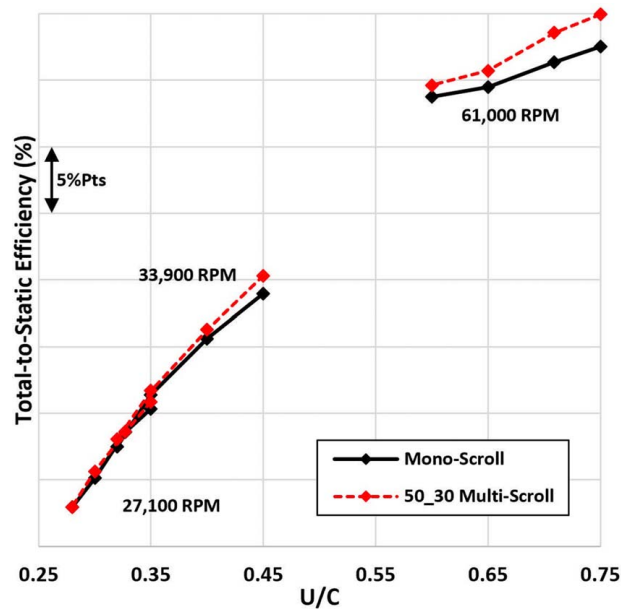


**Fig. 25 Flow cone angle of the Λ60β10 rotor for mono-scroll and multi-scroll configurations at off-design condition**



**Fig. 27 Speedline of 50_30 multi-scroll volute paired with the Λ60β10 rotor**

improvement of 0.5%pts, which was less than the improvement at the design condition. The 50_30 configuration has been investigated at the off-design because the 50_30 volute configuration offered the best overall efficiency gains across both operating conditions. The multi-scroll volute configuration had a higher flowrate between 25% and 50% span compared to the baseline mono-scroll volute (Fig. 23). In this spanwise region, the multi-scroll volute produced a more negative incidence angle (Fig. 24), contributing to improved performance. The flow conditions had improved, which reduced the incidence angle and resulted in an improved flow cone angle in this region, as indicated in Fig. 25. The multi-scroll volute could manipulate the flow to generate a more favorable flow cone angle from 30% to 70% span. Within this region, the flow in the meridional plane was near perpendicular to the rotor LE. The improved flow cone angle was achieved by an increased axial velocity component from 25% to 70% span. This additional region of improved flow angle was absent in the mono-scroll case, mainly due to the reduced axial velocity from 25% to 70% span.

The meridional divider wake contributed to the reduced mass flowrate entering the rotor between 65% and 100% span (Fig. 23). This spanwise region of the LE experienced a more positive incidence angle (Fig. 24); however, the additional separation on the SS was less significant due to the reduced level of mass flow through this region.

A vortex originating from the flow from the backdisk cavity entering the rotor was a significant feature for both mono-scroll and multi-scroll cases and can be clearly identified at the off-design condition in Fig. 26. The flow left the cavity and entered the rotor passage at the hub near the SS, where it moved up from hub to shroud while remaining near the SS. This movement is visible in Fig. 26, where at just 30% chord, this secondary flow generated a vortex at the mid-span region on the SS. This additional vortex mixed with the TLV prior to the TE of the rotor, which increased aerodynamic blockage and increased shroud region losses.

The mono-scroll volute case relied on the exhaust diffuser to some extent to achieve a high level of efficiency at both operating conditions. Calculating the total-to-static efficiency without the exhaust diffuser resulted in the 50_30 multi-scroll case being 1.9%pts more efficient than the mono-scroll at design condition and 1.8%pts at off-design condition. This is an important outcome because most turbocharger applications do not afford the space for an efficient diffuser, so the efficiency values before the diffuser would be a more realistic measure of the advantage in most turbocharger applications.

*4.2.4 Turbine Performance Map.* Figure 27 shows three speed lines simulated for the 50_30 multi-scroll volute configuration with the Λ60β10: 100%, 56%, and 44% of design speed. The multi-scroll case was capable of matching, if not improving, the efficiency compared to the baseline mono-scroll case. The maximum efficiency increase was at the maximum speed, where an improvement of 2.4%pts was achieved. At the most extreme off-design condition, the multi-scroll volute matched the efficiency of the mono-scroll baseline.

# 5 Conclusion

Multi-scroll volutes are able to generate a non-uniform spanwise flow at the inlet of a mixed flow turbine rotor, which has the potential to be used for improving the rotor flow field by reducing incidence near the rotor hub. However, the additional losses associated with the divider wake of the multi-scroll volute could outweigh any benefits within the rotor.

In a numerical study, two mixed flow rotors were studied to investigate the impact of a design matrix of multi-scroll volutes. One rotor had a 30-deg cone angle (Λ30β30), and the other had a 60-deg cone angle (Λ60β10). A wide range of volute geometries were evaluated with highly non-symmetric area distributions between the two limbs.

The study showed significant efficiency benefits for the Λ60β10 rotor, but the efficiency deteriorated when the Λ30β30 rotor was used with a multi-scroll volute, compared to the baseline mono-scroll volute. The Λ60β10 rotor achieved efficiency improvements of up to 2.2%pts at design operating condition and 0.5%pts at off-design condition. The efficiency improvements arose because of the significantly non-uniform flow field that was produced by the multi-scroll volutes across the span of the rotor leading edge. For certain volutes, this manipulated the flow field and particularly the incidence angle at the hub to reduce suction side separation and subsequent loss structures in the rotor passage. The multi-scroll volute biased more mass flow toward the hub of the rotor inlet and away from the shroud region.

The Λ60β10 rotor with the multi-scroll volute achieved improved performance across a full operating map with a range of speeds covering U/C$_{is}$ values between 0.28 and 0.75.

The Λ30β30 rotor did not achieve any performance improvement from the 24 different multi-scroll volute geometries simulated. This was because the 30 deg cone angle rotor did not suffer such severe variation of incidence across the leading edge in the baseline configuration, and the non-uniform flow field from the multi-scroll volutes was not able to yield any improvement in incidence.

Therefore, the potential for a mixed flow turbine to benefit from the non-uniform flow field from a non-symmetric multi-scroll volute was strongly dependent on the cone angle of the turbine. A large cone angle rotor (closer to an axial turbine geometry) could benefit from a multi-scroll turbine to improve incidence distribution and efficiency. A small cone angle rotor (closer to a radial turbine geometry) did not achieve any benefit.

# Conflict of Interest

There are no conflicts of interest.

# Data Availability Statement

The authors attest that all data for this study are included in the paper.

# Nomenclature

## Locations

1 = volute inlet
2 = volute outlet/rotor inlet
3 = rotor outlet/diffuser inlet
4 = diffuser outlet

## Variables

$i$ = incidence angle
$p$ = apparent order of convergence
$P$ = pressure
$T$ = temperature
$U$ = blade tip speed
$\dot{m}$ = mass flow rate
$e_a$ = approximate relative error

$r_f$ = refinement factor
$C_{is}$ = isentropic spouting velocity
$\eta_{TS}$ = total-to-static efficiency
$U/C_{is}$ = velocity ratio
$\%FA_{Hub}$ = percentage of total flow area at hub
$\%OA_{Hub}$ = percentage of total outlet area at hub
$\beta$ = blade inlet angle
$\lambda$ = flow cone angle
$\Lambda$ = blade cone angle
$\Phi$ = blade camber angle

## Abbreviations

$A/r$ = ratio of cross-sectional area to centroid radius
FA = flow area
FOS = factor of safety
GCI = Grid Convergence Index
GGI = general grid interface
LE = leading edge
MFP = mass flow parameter, where $\text{MFP} = \dfrac{\dot{m}\sqrt{T_{01}}}{\dfrac{P_{01}}{P_3}}$
MFT = mixed flow turbine
OA = outlet area
PS = pressure surface
RANS = Reynolds-averaged Navier–Stokes
SS = suction surface
SST = shear stress transport
TE = trailing edge
TLV = tip leakage vortex

## References

[1] Whitfield, A., and Baines, N. C., 1990, *Design of Radial Turbomachines*, John Wiley & Sons, Harlow, Essex, UK.
[2] Roclawski, H., Böhle, M., and Gugau, M., 2012, "Multidisciplinary Design Optimization of a Mixed Flow Turbine Wheel," Proceedings of the ASME Turbo Expo, ASME Paper No. GT2012-68233.
[3] Leonard, T., Spence, S., Starke, A., and Filsinger, D., 2019, "Numerical and Experimental Investigation of the Impact of Mixed Flow Turbine Inlet Cone Angle and Inlet Blade Angle," ASME J. Turbomach., **141**(8), p. 081001.
[4] Baines, N. C., and Yeo, J., 1990, "Pulsating Flow Behaviour in a Twin Entry Vaneless Radial Inflow Turbine," Proceedings of the Institution of Mechanical Engineers, 4th International Conference on Turbochargers and Turbocharging, London, UK, May 22–24, pp. 113–122.
[5] Abidat, M., Baines, N. C., and Firth, M. R., 1992, "Design of a Highly Loaded Mixed Flow Turbine," Proc. Inst. Mech. Eng. A: J. Power Energy, **206**(2), pp. 95–107.
[6] Arcoumanis, C., Martinez-Botas, R. F., Nouri, J. M., and Su, C. C., 1997, "Inlet and Exit Flow Characteristics of Mixed Flow Turbines," Int. J. Rotating Mach., **3**(4), pp. 277–293.
[7] Lee, S. P., Jupp, M. L., Nickson, A. K., and Allport, J. M., 2017, "Analysis of a Tilted Turbine Housing Volute Design Under Pulsating Inlet Conditions," Proceedings of the ASME Turbo Expo, Charlotte, NC, June 26–30.
[8] Lee, S. P., Barrans, S. M., Jupp, M. L., and Nickson, A. K., 2018, "Investigation Into the Impact of Span-Wise Flow Distribution on the Performance of a Mixed Flow Turbine," Proceedings of the ASME Turbo Expo, Oslo, Norway, June 11–15.
[9] Morrison, R., Spence, S., Kim, S., Filsinger, D., and Leonard, T., 2016, "Investigation of the Effects of Flow Conditions at Rotor Inlet on Mixed Flow Turbine Performance for Automotive Applications," NLETT Turbocharging Seminar, Tianjin, China, Sept. 21–22, pp. 1–12.
[10] Morrison, R., Spence, S., Kim, S. I., Leonard, T., and Starke, A., 2020, "Evaluating the Use of Leaned Stator Vanes to Produce a Non-Uniform Flow Distribution Across the Inlet Span of a Mixed Flow Turbine Rotor," ASME J. Turbomach., **142**(12), p. 121001.
[11] Morrison, R., Stuart, C., Kim, S. I., Spence, S., Starke, A., and Leonard, T., 2023, "Investigation of a Novel Turbine Housing to Produce a Non-Uniform Spanwise Flow Field at the Inlet to a Mixed Flow Turbine and Provide Variable Geometry Capabilities," ASME J. Turbomach., **145**(6), p. 061013.
[12] Capobianco, M., and Gambarotta, A., 1993, "Performance of a Twin-Entry Automotive Turbocharger Turbine," Proceedings of the 16th Annual ASME Energy-Sources Technology Conference and Exhibition, Houston, TX, Jan. 31– Feb. 4, pp. 1–10.
[13] Walkingshaw, J., Spence, S., Ehrhard, J., and Thornhill, D., 2013, "An Experimental Assessment of the Effects of Stator Vane Tip Clearance Location and Back Swept Blading on an Automotive Variable Geometry Turbocharger," ASME J. Turbomach., **136**(6), p. 061001.
[14] ANSYS Inc., 2019, CFX Solver Theory Guide, ANSYS, p. 59. Release 2019-R3.
[15] Menter, F. R., 1993, "Zonal Two Equation k-ω Turbulence Models for Aerodynamic Flows," AIAA Paper No. 93-2906.
[16] Menter, F. R., 1994, "Two-Equation Eddy-Viscosity Turbulence Models for Engineering Applications," AIAA J., **32**(8), pp. 1598–1605.
[17] Roache, P. J., 1998, *Verification and Validation in Computational Science and Engineering*, Hermosa Publishers, Albuquerque, NM.
[18] Celik, I. B., Ghia, U., Roache, P. J., Freitas, C. J., Coleman, H., and Raad, P. E., 2008, "Procedure for Estimation and Reporting of Uncertainty Due to Discretization in CFD Applications," ASME J. Fluids Eng., **130**(7), p. 078001.
[19] Kock, F., and Herwig, H., 2005, "Entropy Production Calculation for Turbulent Shear Flows and Their Implementation in CFD Codes," Int. J. Heat Fluid Flow, **26**(4), pp. 672–680.